
Quantification and Visualization of Defects of the Functional Dopaminergic System Using an Automatic Algorithm

Jan B.A. Habraken, Jan Booij, Piotr Slomka, Ellinor Busemann Sokole and Eric A. van Royen

Graduate School of Neurosciences Amsterdam, Department of Nuclear Medicine, Academic Medical Center, University of Amsterdam, Amsterdam, The Netherlands; and Department of Diagnostic Radiology and Nuclear Medicine, University of Western Ontario and Victoria Hospital, London, Ontario, Canada

In SPECT, the binding of radiotracers in brain areas is usually assessed by manual positioning of regions of interest (ROIs). The disadvantages of this method are that it is an observer-dependent procedure and that it may not be sensitive for assessing defects significantly smaller than the ROI. To circumvent these limitations, we developed a fully automatic three-dimensional technique that quantifies neuronal radiotracer binding on a voxel-by-voxel basis. **Methods:** To build a model of normal ^{123}I -labeled *N*- ω -fluoropropyl-2 β -carbomethoxy-3 β -(4-iodophenyl)nortropane (FPCIT) binding, 17 studies of healthy volunteers were registered to the same orientation. After registration, the specific-to-nonspecific binding ratio was calculated for each voxel of the striatal volumes of interest (VOIs). The mean and SD of that binding ratio were then calculated on a voxel-by-voxel basis. For the analysis of 10 healthy volunteer studies (control group) and 21 studies of drug-naive patients with Parkinson's disease, the registration and calculation of the specific-to-nonspecific [^{123}I]FPCIT binding ratio were performed by the same method. Subsequently, a voxel of the striata was classified as a diminished [^{123}I]FPCIT binding ratio if its value was lower than the mean $-2 \times \text{SD}$. For each subject, the defect size, the relative number of voxels with a diminished binding ratio and the binding ratio of the whole striatal VOIs were calculated and compared with the binding ratio as assessed by the traditional ROI method. **Results:** The results of the automatic method correlated significantly with the results of the traditional ROI method. Furthermore, for the ipsilateral side, the automatically calculated defect size had less overlap between the patient and the control group than the traditionally calculated binding ratio. **Conclusion:** The method presented quantifies [^{123}I]FPCIT binding ratio automatically on a voxel-by-voxel basis, by comparison with a model of healthy volunteers. We have shown that it is appropriate to use the automatic method as a replacement for the traditional manual method, which enables us to study the localized dopaminergic degeneration process in Parkinson's disease more precisely and without any inter- or intraobserver variability.

Key Words: ^{123}I -labeled *N*- ω -fluoropropyl-2 β -carbomethoxy-3 β -(4-iodophenyl)nortropane; SPECT; three-dimensional; automatic quantification

J Nucl Med 1999; 40:1091-1097

The main neuropathologic feature in Parkinson's disease is a severe degeneration of dopaminergic neurons in the substantia nigra, resulting in a loss of dopamine transporters in the striatum (1,2). PET and SPECT techniques now provide unique opportunities for examining these transporters in the human brain in vivo. Various radiotracers for imaging of the dopamine transporter, by means of PET and SPECT, have been introduced. In particular, several cocaine analogs, as PET and SPECT radiotracers, have shown to be successful agents for imaging the dopamine transporter (3,4). Several imaging studies have shown pronounced decline of striatal dopamine transporter binding in patients with Parkinson's disease (3-6). The loss of dopamine transporter binding in patients with Parkinson's disease is typically more pronounced in subregions of the striatum.

In general, on SPECT, the binding of radiotracers in brain areas, known to be representative of specific and nonspecific binding, is assessed by manual positioning of regions of interest (ROIs). Quantification of dopamine transporters is routinely based on a ratio-equilibrium analysis, in which the ratio of radioactivity measured in the striatum to that in a brain area, representative of nonspecific binding, is determined (7). Positioning of ROIs can be performed manually, on one or more slices of the SPECT study. A coregistered MRI study can be used for more optimal positioning (5). Even if one uses ROIs of a standard size and shape (8,9), the positioning remains manual and is therefore an observer-dependent procedure. Another disadvantage of quantification using ROIs is that it may not be sensitive for assessing disturbances in subregions of the striatum that are significantly smaller than the ROI. To circumvent these limitations, we developed a fully three-dimensional automatic, observer-independent technique that quantifies neuronal radiotracer binding on a voxel-by-voxel basis (voxel-based automatic neuronal quantification [VANQ]). From studies performed in healthy volunteers, a three-dimensional model was made to assess the physiological variation in dopamine transporter binding on a voxel-by-voxel basis. VANQ calculated, completely automatically, the specific-to-nonspecific binding ratio and the defect size of the dopaminergic system

Received Jun. 22, 1998; revision accepted Nov. 5, 1998.
For correspondence or reprints contact: Jan B.A. Habraken, MSc, Department of Nuclear Medicine, Academic Medical Center, Meibergdreef 9, 1105 AZ Amsterdam, The Netherlands.

for the left and right striatum. We tested this new technique for the analysis of dopamine transporter binding in groups of healthy volunteers and patients with Parkinson's disease, using ^{123}I -labeled *N*- ω -fluoropropyl-2 β -carbomethoxy-3 β -(4-iodophenyl)nortropane (FPCIT) as the radioligand.

MATERIALS AND METHODS

Subjects

Twenty-seven healthy volunteers (12 men, 15 women) and 21 patients (15 men, 6 women) with clinically established Parkinson's disease, according to the U.K. Parkinson's Disease Society Brain Bank criteria, were selected. The healthy volunteers and patients with Parkinson's disease were drug-naïve at the time of the study. The medical ethics committee gave permission for the study. All participants gave their written informed consent. The stage of illness of the patients varied from I to III on the Hoehn and Yahr staging scale (early Parkinson's disease) (10). Data of the ROI analysis in patients have been published (11). The healthy volunteers had no evidence of neurologic or psychiatric disease. There were no significant age differences between the healthy volunteers (mean age 57.4 ± 14.7 y) and patients with Parkinson's disease (mean age 55.5 ± 9.7 y). SPECT data obtained in 17 healthy volunteers were used to build a model of normal striatal [^{123}I]FPCIT binding (model group). SPECT data obtained in 10 other healthy volunteers were used to create a control group.

SPECT System and Reconstruction

Three hours after the injection of approximately 111 MBq [^{123}I]FPCIT, studies were acquired in all subjects with a brain dedicated SPECT system (the Strichman Medical Equipment 810X; Strichman Medical Equipment, Inc., Medfield, MA) linked to a Macintosh II Apple computer (Apple Computer, Inc., Cupertino, CA). This system scans the volume slice after slice with 12 focal-point detectors. For every slice, each detector performs a three-dimensional rectilinear translation along its orthogonal direction in nine lines (128 pixels in line), scanning half of the volume nearest to it (12). The transaxial resolution of the system is 7.6 mm full width at half maximum (FWHM) of a line source in air, and the axial resolution is 13.5 mm FWHM (13). Phantom studies, performed with this SPECT system, have shown that the measured counts per pixel have a linear relationship with the real concentration of radioactivity (14,15).

Reconstruction of raw data was performed slice after slice with an iterative algorithm (12). Linear attenuation was performed with an attenuation coefficient of 0.11 cm^{-1} within an ellipse drawn around the head. No scatter correction was applied. Images were reconstructed into 64×64 pixel slices, 3.175 mm per pixel, 5 mm slice distance.

Traditional Manual Data Analysis Method, Regions of Interest Method

In the traditional manual analysis method, two axial slices with the highest striatal activity were selected and a standard template, with ROIs constructed manually according to a stereotactic atlas (16), was applied. The template was positioned manually, without changing the size and shape of the ROIs, and the specific-to-nonspecific [^{123}I]FPCIT binding ratio was then calculated as:

$$R^M = \frac{\text{STR} - \text{OCC}}{\text{OCC}}, \quad \text{Eq. 1}$$

where STR represents the mean value of activity (counts per second per pixel) in the striatal ROI and OCC depicts the mean value of activity in the occipital cortex ROI (nonspecific binding).

Voxel-Based Automatic Neuronal Quantification Method

The automatic data analysis method VANQ is based on a map of volumes of interest (VOI-map) and a reference model. The generation of the reference model from studies of healthy volunteers (A) is described below in steps A1 to A3, and the three-dimensional quantification (B) is explained in steps B1 to B3.

Creating the Reference Model of Normal Striatal Binding

Step A1: Registration Process. The VOIs of the left and the right striatum (VOI_0 and VOI_1 , respectively) and the left and right occipital cortex (VOI_2 and VOI_3 , respectively) were stored in a VOI-map. The VOI-map was created according to a standard stereotactic atlas (16), as described previously (17). A transformation, T_i , with three rotation parameters and three translation parameters was allocated for each VOI_i , as symbolically indicated by the arrows in Figure 1. Scaling parameters were not included in the transformation, on the basis of the assumption that the size of the VOIs was comparable for each subject (18). Each VOI was positioned automatically on the image by adjusting the rotation and translation parameters by simplex method to minimize a mathematical cost function, C_i (19). However, the definition of the cost function for VOI_0 and VOI_1 (striatal volumes) differed from that for VOI_2 and VOI_3 (occipital volumes). To position VOI_0 and VOI_1 optimally in an area of striatal radioactivity, the cost function for VOI_0 and VOI_1 was defined in a way that minimization of the function results in a maximization of the total counts in these VOIs. Therefore, the cost function, for these VOIs was defined to be the negative value of the summed counts in the VOI_i after the transformation T_i :

$$C_{i=0,1} = - \text{totalcounts}_i = - \sum_{r_{\text{VOI}_i}} S(T_i r_{\text{VOI}_i}), \quad \text{Eq. 2}$$

where r_{VOI_i} is a coordinate of a voxel within VOI_i as specified by the VOI-map, $T_i r_{\text{VOI}_i}$ is the coordinate after the transformation T_i and $S(T_i r_{\text{VOI}_i})$ represents the value of the study S at coordinate $T_i r_{\text{VOI}_i}$ in counts per second. The adjustment of T_i for positioning of VOI_0 and VOI_1 was restricted by the requirement that VOI_0 must be positioned on the image left of VOI_1 .

To position VOI_2 and VOI_3 optimally in a brain area known to be representative of nonspecific [^{123}I]FPCIT activity (occipital cortex), the cost function for VOI_2 and VOI_3 was defined in a way that the homogeneity of counts within the VOI was maximized. The cost function for these VOIs therefore equals the variance (SD^2) of the counts within the VOI divided by the total counts in the VOI:

$$C_{i=2,3} = \frac{\text{SD}_i^2}{\text{totalcounts}_i} = \frac{\sum_{r_{\text{VOI}_i}} S(T_i r_{\text{VOI}_i})^2}{n_i} - \left(\frac{\sum_{r_{\text{VOI}_i}} S(T_i r_{\text{VOI}_i})}{n_i} \right)^2, \quad \text{Eq. 3}$$

where n_i represents the number of voxels within VOI_i . The adjustment of T_i for positioning of VOI_2 and VOI_3 was restricted by the requirement that they must be positioned on the image inferior to VOI_0 and VOI_1 , and that VOI_2 must be positioned left of VOI_3 .

Step A2: Calculation of Specific-to-Nonspecific Binding Ratio. After optimization of the transformation parameters, the average

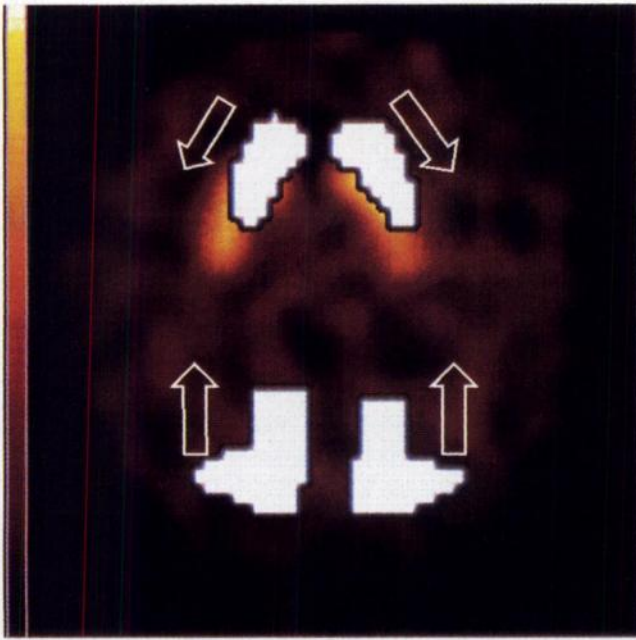


FIGURE 1. Registration process of VOI-map and study, three-dimensional process is symbolically presented in two dimensions, each arrow is coupled with VOI and represents transformation with rotation parameters and translation parameters.

nonspecific [¹²³I]FPCIT binding was calculated using the information within the occipital VOIs:

$$AVE_{\text{nonspecific}} = \frac{\text{totalcounts}_2 + \text{totalcounts}_3}{n_2 + n_3}, \quad \text{Eq. 4}$$

where n_2 and n_3 are the total number of voxels of the left and right occipital cortex and totalcounts is the total number of counts in these VOIs. For each voxel in the striatal volumes ($\text{VOI}_i = 0,1$), the ratio of the specific-to-nonspecific binding was calculated and remapped onto the VOI-map:

$$S_{\text{ratio}}(r_{\text{VOI}_i=0,1}) = \frac{S(T_i r_{\text{VOI}_i}) - AVE_{\text{nonspecific}}}{AVE_{\text{nonspecific}}}. \quad \text{Eq. 5}$$

The resulting study S_{ratio} represents the striatal binding ratio within the coordinates of the VOI-map.

Step A3: Calculation of the Mean and the SD Model. The registration and calculation steps were successfully performed on 16 of the 17 healthy volunteer studies. In one study, three-dimensional

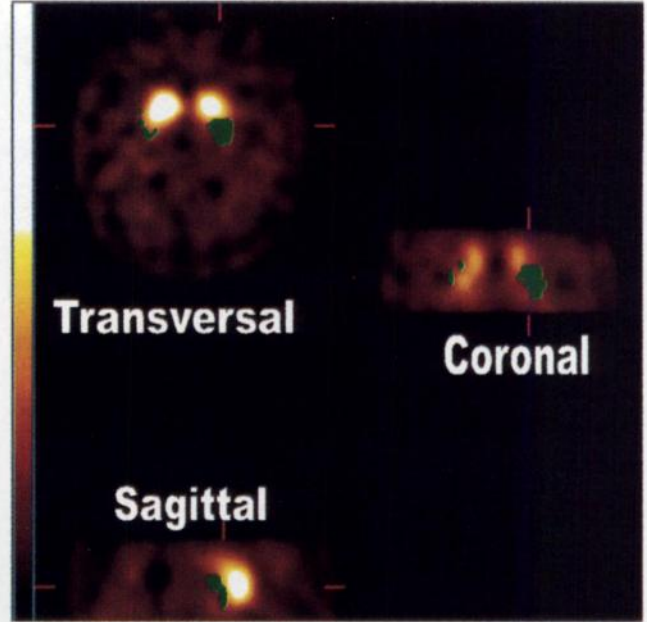


FIGURE 3. Patient study 14 with volumes representing loss of striatal [¹²³I]FPCIT binding shown in green.

registration was not possible because not all slices with striatal activity had been acquired. Because all 16 studies were aligned in the orientation of the VOI-map, we could calculate the mean and SD of the [¹²³I]FPCIT binding ratio for each striatal voxel:

$$\text{mean}(r_{\text{VOI}_i=0,1}) = \frac{\sum_{s=1}^{N_{\text{studies}}} S_{\text{ratio}}(r_{\text{VOI}_i})}{N_{\text{studies}}} \quad \text{Eq. 6}$$

$$SD(r_{\text{VOI}_i=0,1}) =$$

$$\sqrt{\frac{\sum_{s=1}^{N_{\text{studies}}} S_{\text{ratio}}^2(r_{\text{VOI}_i}) - \frac{1}{N_{\text{studies}}} \left(\sum_{s=1}^{N_{\text{studies}}} S_{\text{ratio}}(r_{\text{VOI}_i}) \right)^2}{N_{\text{studies}} - 1}}, \quad \text{Eq. 7}$$

where $r_{\text{VOI}_i = 0,1}$ is a coordinate of a striatal VOI and N_{studies} is the number of included normal studies (16). Our completed model consists of a three-dimensional mean and SD representation of the [¹²³I]FPCIT binding ratio (Fig. 2).

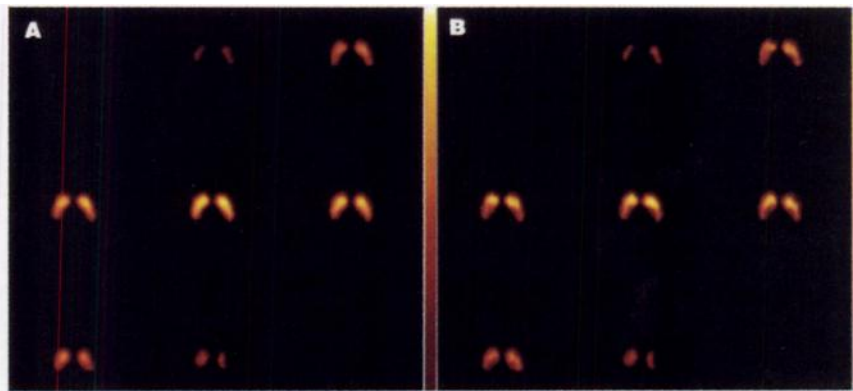


FIGURE 2. Transverse slices of [¹²³I]FPCIT binding ratio model. Mean (A) and SD (B) are presented.

Three-Dimensional Quantification of [¹²³I]FPCIT Binding Using the Model

After the creation of the three-dimensional model of normal striatal [¹²³I]FPCIT binding ratios, we were able to quantify [¹²³I]FPCIT studies of healthy volunteers and patients on a detailed voxel-by-voxel basis. The registration of each study with the VOI-map and the calculation of specific-to-nonspecific binding ratio on a voxel-by-voxel basis were performed in steps B1 and B2, which were identical to steps A1 and A2. This resulted in a binding ratio study S_{ratio} , aligned to the VOI-map, that could be compared directly with the mean and SD model.

Step B3: Calculation of Defects. Because the study S_{ratio} and the model were matched, we were able to perform quantification on a voxel-by-voxel basis. A voxel of the striata was specified to have a diminished [¹²³I]FPCIT binding ratio if:

$$S_{ratio}(r_{VOI_{i=0.1}}) < \text{mean}(r_{VOI_i}) - 2 \times SD(r_{VOI_i}). \quad \text{Eq. 8}$$

For the purpose of visualization of defects, volumes that represented diminished striatal [¹²³I]FPCIT binding were now reoriented over the inverse transformation T_i^{-1} to the original study (S) orientation (Fig. 3). The relative defect size (DS) was calculated separately for left and right striatum:

$$DS_{VOI_{i=0.1}}(\%) = \frac{n_{\text{defect}_{VOI_i}}}{n_{VOI_i}} \times 100\%, \quad \text{Eq. 9}$$

where $n_{\text{defect}_{VOI}}$ is the number of voxels, which complies with equation 8, and n_{VOI} is the total number of voxels of the specified VOI.

In addition to the defect size, the average binding ratio for the left and the right striatum was calculated:

$$R^A_{VOI_{i=0.1}} = \frac{AVE_{VOI_{i=0.1}} - AVE_{\text{nonspecific}}}{AVE_{\text{nonspecific}}}, \quad \text{Eq. 10}$$

where $R^A_{VOI_i}$ represents the average counts per voxel within the striatal VOI_i . All studies were analyzed with the automatic algorithm, using the same parameters. No user intervention was required.

Statistical Analysis

Student *t* tests for independent samples were used to test differences between the control group and the patient group on statistical significance. Linear regression was used to examine the relationship between measures from the traditional ROI and the currently developed three-dimensional automatic technique. All tests were two-tailed with the accepted level of significance at $P < 0.01$.

RESULTS

Table 1 shows the values obtained by the traditional manual method, the binding ratio R^M , and by the automatic method, the binding ratio R^A , and the DS, for each patient,

TABLE 1
(Striatal-Occipital)/Occipital Binding Ratio as Calculated by Manual Method and Binding Ratio and Defect Size as Calculated by Automatic Algorithm, Per Subject, of Ipsilateral and Contralateral Striatum

| | Model group | | | Control group | | | Patient group | | |
|----|---------------------------|-----------|---------|---------------------------|-----------|---------|---------------------------|-----------|-----------|
| | Contralateral/ipsilateral | | | Contralateral/ipsilateral | | | Contralateral/ipsilateral | | |
| | R^M | R^A | DS (%) | R^M | R^A | DS (%) | R^M | R^A | DS (%) |
| 1 | 1.55/1.45 | 1.54/1.52 | 3.9/3.6 | 2.46/2.39 | 2.67/2.63 | 0.3/0.0 | 1.88/2.51 | 1.99/2.54 | 3.0/0.0 |
| 2 | 2.29/2.29 | 2.18/2.14 | 0.0/0.0 | 3.15/3.03 | 2.47/2.59 | 0.0/0.3 | 0.68/0.87 | 0.79/1.02 | 57.6/38.6 |
| 3 | 2.37/2.32 | 2.06/2.11 | 0.0/0.0 | 2.07/1.93 | 2.32/2.26 | 1.0/0.0 | 0.85/0.85 | 0.82/1.00 | 50.0/38.3 |
| 4 | 2.39/2.39 | 2.56/2.41 | 0.0/0.0 | 2.36/2.27 | 2.47/2.41 | 0.0/0.0 | 1.33/1.94 | 1.39/1.88 | 32.5/8.6 |
| 5 | 1.53/1.40 | 1.69/1.71 | 1.6/2.3 | 2.56/2.61 | 2.76/2.86 | 0.0/0.0 | 1.78/2.15 | 2.05/2.45 | 23.1/1.6 |
| 6 | 1.85/1.94 | 2.12/2.07 | 0.0/0.0 | 2.21/2.21 | 2.65/2.61 | 0.3/0.7 | 1.11/1.33 | 1.18/1.42 | 38.6/22.4 |
| 7 | 5.00/4.20 | 4.54/4.48 | 0.0/0.0 | 2.13/2.25 | 2.39/2.42 | 0.3/0.3 | 0.75/1.10 | 0.94/1.28 | 41.4/27.6 |
| 8 | 2.19/2.14 | 2.11/2.09 | 0.0/0.0 | 1.91/1.91 | 2.15/2.03 | 1.0/2.9 | 0.96/1.11 | 0.92/1.21 | 47.7/28.6 |
| 9 | 2.43/2.71 | 2.40/2.63 | 0.0/0.0 | 2.37/2.37 | 2.38/2.51 | 0.0/0.0 | 1.42/1.56 | 1.62/1.74 | 19.7/14.9 |
| 10 | 3.55/3.16 | 3.75/3.45 | 0.0/0.0 | | | | 1.41/1.94 | 1.60/2.01 | 19.5/5.3 |
| 11 | 2.21/2.11 | 2.30/2.20 | 0.7/0.3 | | | | 1.13/1.55 | 1.11/1.54 | 39.6/7.6 |
| 12 | 2.09/2.09 | 2.38/2.37 | 0.0/0.0 | | | | 0.77/0.95 | 0.69/0.94 | 62.3/45.7 |
| 13 | 2.86/2.79 | 3.14/3.16 | 1.6/0.0 | | | | 0.84/1.28 | 1.05/1.48 | 44.5/16.8 |
| 14 | 2.47/2.28 | 2.82/2.64 | 0.0/0.3 | | | | 1.71/2.07 | 1.73/2.18 | 19.1/9.4 |
| 15 | 2.81/2.86 | 2.68/2.76 | 0.0/0.0 | | | | 0.89/1.00 | 1.06/1.06 | 37.7/31.9 |
| 16 | 2.18/2.14 | 2.20/2.11 | 0.7/0.3 | | | | 0.92/1.29 | 1.13/1.47 | 33.8/11.5 |
| 17 | | | | | | | 1.48/1.96 | 1.80/2.30 | 17.2/7.2 |
| 18 | | | | | | | 0.90/1.33 | 0.92/1.51 | 37.2/14.3 |
| 19 | | | | | | | 0.86/1.24 | 0.98/1.54 | 39.8/17.9 |
| 20 | | | | | | | 0.96/1.00 | 1.17/1.27 | 30.6/31.5 |
| 21 | | | | | | | 1.22/1.53 | 1.27/1.76 | 37.2/11.7 |

For patients with Parkinson's disease, contralateral was defined as the side opposite that of initial presentation of motor signs; for healthy volunteers, contralateral was arbitrarily assigned to the left striatum.

R^M = manual method; R^A = automatic algorithm; DS = defect size.

for the contralateral and ipsilateral striatum. For patients with Parkinson's disease, contralateral was defined as the side opposite that of initial presentation of motor signs. For healthy volunteers, contralateral was arbitrarily assigned to the left striatum. The automatic algorithm failed on one study of the control group, due to an insufficient number of acquired slices ($n = 9$).

All three parameters (R^M , R^A and DS) showed a significant ($P \leq 0.001$) loss of striatal binding in the patient group compared with the control group, on both the contralateral and ipsilateral sides. A significant and positive correlation was found between the ratios R^M and R^A , for patients ($n = 21$, ipsilateral $r = 0.974$, $P \leq 0.001$; contralateral $r = 0.964$, $P \leq 0.001$), as well as healthy volunteers (model plus control group, $n = 25$, ipsilateral $r = 0.936$, $P \leq 0.001$; contralateral $r = 0.928$, $P \leq 0.001$). For the patient group, a significant and negative correlation was found between R^M and DSs ($n = 21$, ipsilateral $r = -0.887$, $P \leq 0.001$; contralateral $r = -0.871$, $P \leq 0.001$). As anticipated, the DSs, measured in the healthy volunteers, were equal or close to zero. Therefore, for the control and the model group, the correlation between R^M and DS was low; however, on the side defined as ipsilateral, this correlation was proven to be significant (model plus control group, $n = 25$, ipsilateral $r = -0.529$, $P = 0.007$; contralateral $r = -0.389$, $P = 0.055$).

Figure 4 shows the values of DS plotted against R^M for the contralateral striatal side for both control and patient groups. For R^M , the data of 3 patients nearly overlap the data of the control group. For the automatically calculated DS, the

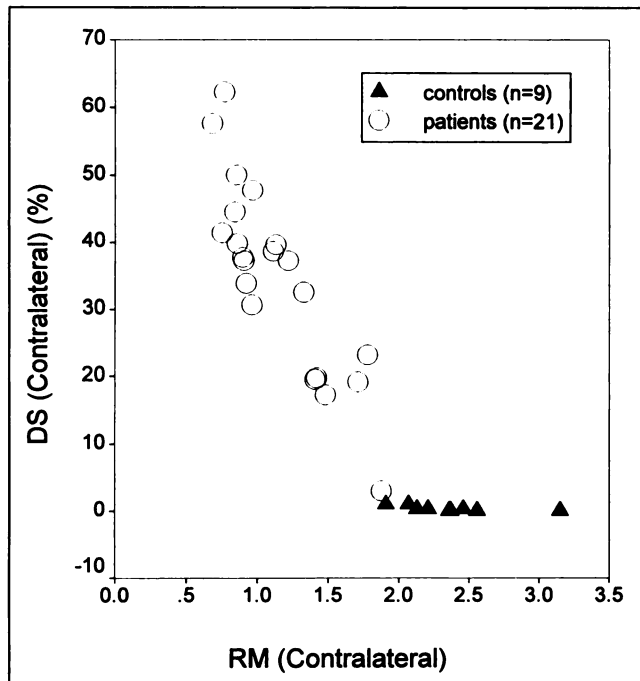


FIGURE 4. DS plotted against R^M for contralateral side, for both control and patient groups.

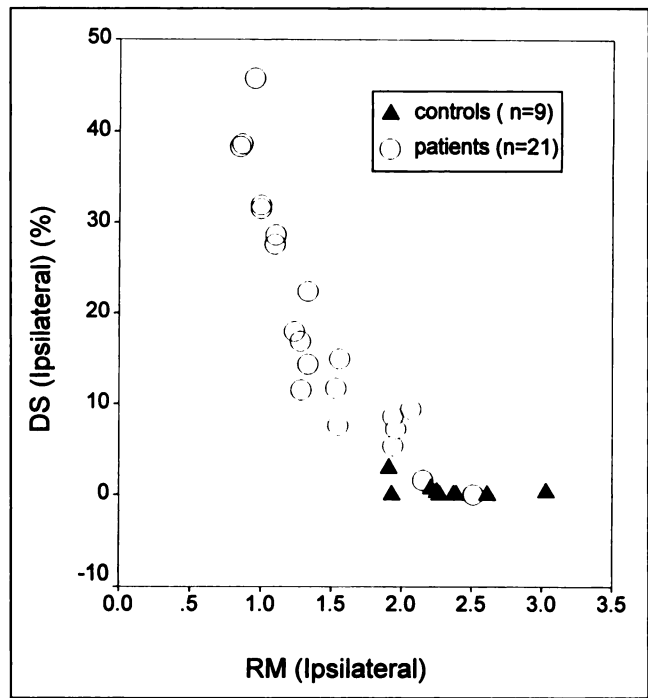


FIGURE 5. DS plotted against R^M for ipsilateral side, for both control and patient groups.

data of only 1 patient nearly overlaps the data of the control group. However, for both R^M and DS, there was quantitatively no overlap between data obtained in the patient and control group on the contralateral side; a 100% discrimination between patient and control data could be made with each parameter, R^M and DS, considered separately. Figure 5 shows the values of DS plotted against R^M for the ipsilateral striatal side, for both control and patient groups. The data in this figure show an overlap between data obtained in the patient and control groups, for both the parameters R^M and DS. However, the overlap of data is less for DS than for R^M . Data of 6 individual patients, obtained with the R^M parameter, and data of 2 individual patients, obtained with the DS parameter, fell within the control range.

DISCUSSION

In general, quantitative measurement of dopamine transporters in SPECT is based on a ratio analysis of the concentration of radioactivity in the striatum to that in a nonspecific brain region (20,21). Serious drawbacks of this method are that the method is observer dependent and that the quantification is not on a pixel-by-pixel or a voxel-by-voxel basis. In an effort to circumvent these limitations, several methods have been evaluated. Friston et al. (22) used the statistical parametric mapping (SPM) method to compare PET studies that are imaged under different conditions on a voxel-by-voxel basis. This implementation of SPM examines whether local variations of a parameter under different study conditions are significant, correcting for global changes of the parameter. SPM has also been used for

the detection of regional changes between groups (23,24). Weeks et al. (24) showed that SPM analysis is a more sensitive technique for group-to-group comparison of PET studies than the ROI analysis technique. Several other groups focused on studying differences between groups on a pixel-by-pixel basis (25–28). These methods calculate the mean and the SD of each group on a pixel-by-pixel basis after registration and normalization of the studies. For example, Kuwabara et al. (28) used the pixel-occipital ratio to study differences in FDOPA binding between groups of patients with Parkinson's disease and healthy volunteers. These methods are of scientific interest because they show regional changes between groups. However, for diagnostic studies, data from 1 individual patient have to be compared with data obtained in healthy controls. Consequently, Minoshima et al. (29) demonstrated the use of z-score parameter maps to compare data of an individual patient study with a model of normal volunteers. In this study, each pixel value was automatically normalized to the thalamic activity, and registration of the patient study with the model was performed using linear scaling and nonlinear warping techniques (30). For the automatic quantitative analysis of myocardial perfusion SPECT scans, a comparable technique was developed by Slomka et al. (31,32). This system quantifies an individual patient study on a voxel-by-voxel basis after normalization and registration to a model of normal studies. This approach has shown to be accurate for the interpretation of myocardial SPECT studies and is promising in the automatic quantification of brain blood flow studies but does not provide comparison of a binding parameter as needed for the quantification of brain receptor studies.

Because [¹²³I]FPCIT studies show a high specific binding in striatal areas and, consequently, show a large functional difference between pathologic and normal studies, the linear scaling and nonlinear warping techniques are not optimal for the registration of [¹²³I]FPCIT studies. We therefore developed VANQ and implemented a three-dimensional registration technique that registers each VOI separately. The only limitation of using VANQ compared with the traditional ROI method is that the complete striatal volume has to be acquired. Two of the included studies could not be analyzed automatically for this reason. Because striatal VOIs were positioned in volumes with maximum counts and occipital VOIs in volumes with maximum homogeneity, the result of the registration was in accordance with anatomic and functional knowledge. In this study, we showed that the VANQ technique was able to detect defects of the nigrostriatal system in drug-naive patients with Parkinson's disease. Interestingly, in the patient group, the defect size correlated significantly with the loss of striatal dopamine transporters detected by the traditional ROI method. Because VANQ does not require any user intervention, it does not introduce any interobserver or intraobserver variability.

In this study, we showed bilateral loss of striatal dopamine transporters in patients with early Parkinson's disease using

[¹²³I]FPCIT SPECT. Although it was observed that, on the contralateral side, 3 patients nearly overlapped with control data using the R^M parameter, both parameters R^M and DS discriminated 100% between patient and control data on the contralateral side. However, on the ipsilateral side, the striatal side where Parkinson's disease manifests itself the latest, an overlap between patient and control data was measured for both parameters. Interestingly, the DS of the ipsilateral striatum had less overlap between patients and controls than the binding ratios calculated by the traditional ROI technique. Although this difference cannot be proven to be statistically significant, it supports the hypothesis that a voxel-by-voxel-based technique is more sensitive for the early diagnosis of Parkinson's disease than the ROI analysis technique. A further benefit of using VANQ is that it visualizes exactly which part of the striatum is classified as having a diminished [¹²³I]FPCIT binding, which enables us to study the localized degeneration nigrostriatal dopaminergic process in more detail.

CONCLUSION

Currently, the main output parameters of VANQ are the DSs in left and right striata. However, we wish to investigate the possibilities of subdividing the VOI of the striatum accurately into anatomic subvolumes, such as anterior and posterior putamen and caudate nucleus, to get a more accurate anatomic localization of the quantified defects. During registration, our method assumes that the size of the VOIs is equal for all patients and healthy subjects. This assumption is supported by Bøtcher (18); however, the effect of this assumption on this quantification method needs further study. Our model of normal striatal [¹²³I]FPCIT binding ratio has not considered gender and age dependency. For example, Tissingh et al. (11) recently showed that striatal binding is age dependent. To address this important issue, we must build separate models for male and female patients, which are corrected for dopaminergic degeneration by normal aging, to quantify pathologic degeneration of the dopaminergic system more accurately. Furthermore, future work will focus on using our method for the automatic quantification of other types of brain receptor and transporter studies.

REFERENCES

1. Bernheimer H, Birkmayer W, Hornykiewicz O, Jellinger K, Seitelberger F. Brain dopamine and the syndromes of Parkinson and Huntington. *J Neurol Sci.* 1973;20:415–455.
2. Kaufman MJ, Madras BK. Severe depletion of cocaine recognition sites associated with the dopamine transporter in Parkinson's-diseased striatum. *Synapse.* 1991;9:43–49.
3. Leenders KL, Salmon EP, Tyrrel P, et al. The nigrostriatal dopaminergic system assessed in vivo by positron emission tomography in healthy volunteer subjects and patients with Parkinson's disease. *Arch Neurol.* 1990;47:1290–1298.
4. Innis RB, Seibyl JP, Scanley BE, et al. Single photon emission computed tomographic imaging demonstrates loss of striatal dopamine transporters in Parkinson's disease. *Proc Natl Acad Sci USA.* 1993;90:1165–1169.
5. Ishikawa T, Dhawan V, Kazumata K, et al. Comparative nigrostriatal dopaminergic imaging with iodine-123-βCIT-FP/SPECT and fluorine-18-FDOPA/PET. *J Nucl Med.* 1996;37:1760–1765.

6. Frost JJ, Rosier AJ, Reich SG, et al. Positron emission tomographic imaging of dopamine transporter with ¹¹C-WIN 35,428 reveals marked declines in mild Parkinson's disease. *Ann Neurol.* 1993;34:423-431.
7. Laruelle M, Baldwin RM, Malison RT, et al. SPECT imaging of dopamine and serotonin transporters with [¹²³I]β-CIT: pharmacological characterization of brain uptake in non-human primates. *Synapse.* 1993;13:295-309.
8. Neumeier JL, Wang S, Gao Y, et al. N-ω-fluoroalkyl analogs of (1R)-2β-carbomethoxy-3-β-(4-iodophenyl)-tropane (β-CIT): radiotracers for positron emission tomography and single photon emission computed tomography imaging of dopamine transporters. *J Med Chem.* 1994;37:1558-1561.
9. Booij J, Tissingh G, Boer GJ, et al. [¹²³I]FP-CIT SPECT shows a pronounced decline of striatal dopamine transporter labeling in early and advanced Parkinson's disease. *J Neurol Neurosurg Psychiatry.* 1997;62:133-140.
10. Hoehn MM, Yahr MD. Parkinsonism: onset, progression and mortality. *Neurology.* 1967;17:427-442.
11. Tissingh G, Booij J, Bergmans P, et al. Iodine-123-N-ω-fluoropropyl-2β-carbomethoxy-3-β-(4-iodophenyl)tropane SPECT in healthy controls and early-stage, drug-naive Parkinson's disease. *J Nucl Med.* 1998;39:1143-1148.
12. Stoddart HA, Stoddart HF. New multi-dimensional reconstructions for the 12-detector, scanned focal point, single-photon tomograph. *Phys Med Biol.* 1992;37:579-586.
13. Vermeulen RJ, Wolters EC, Tissingh G, et al. Evaluation of [¹²³I]β-CIT binding with SPECT in controls, early and late Parkinson's disease. *Nucl Med Biol.* 1995;22:985-991.
14. Innis RB, Al-Tikriti MS, Zoghbi SS, et al. SPECT imaging of the benzodiazepine receptor: feasibility of in vivo potency measurements from stepwise displacement curves. *J Nucl Med.* 1991;32:1754-1761.
15. Verhoeff NPLG, Kapucu O, Sokole-Busemann E, et al. Estimation of dopamine D2 receptor binding potential in the striatum with iodine-123-IBZM SPECT: technical and interobserver variability. *J Nucl Med.* 1993;34:2076-2084.
16. Matsui T, Hirano A. *An Atlas of the Human Brain for Computerized Tomography.* Stuttgart, Germany: Gustav Fisher Verlag; 1978.
17. Booij J, Habraken JBA, Bergmans P, et al. Imaging of dopamine transporters with iodine-123-FP-CIT SPECT in healthy controls and patients with Parkinson's disease. *J Nucl Med.* 1998;39:1879-1884.
18. Bøtcher J. Morphology of the basal ganglia in Parkinson's disease. *Acta Neurol Scand.* 1975; 62(suppl):1187.
19. Press WH, Flannery BP, Teukolsky SA, Vetterling WT. *Numerical Recipes: The Art of Scientific Computing.* New York, NY: Cambridge University Press; 1986:289-293.
20. Seibyl JP, Laruelle M, Dyck CH. Reproducibility of iodine-123-β-CIT SPECT brain measurements of dopamine transporters. *J Nucl Med.* 1996;37:222-228.
21. Assenbaum S, Brücke T, Pirker W, et al. Imaging of dopamine transporters with iodine 123-β-CIT and SPECT in Parkinson's disease. *J Nucl Med.* 1997;38:1-6.
22. Friston KJ, Frith CD, Liddle PF, et al. The relationship between global and local changes in PET scans. *J Cereb Blood Flow Metab.* 1990;10:458-466.
23. Piccini P, Weeks RA, Brooks DJ. Alterations in opioid receptor binding in Parkinson's disease patients with levodopa-induced dyskinesias. *Ann Neurol.* 1997;42:720-726.
24. Weeks RA, Cunningham VJ, Piccini P, et al. ¹¹C-diprenorphine binding in Huntington's disease: a comparison of interest analysis with statistical parametric mapping. *J Cereb Blood Flow Metab.* 1997;17:943-949.
25. Borghet T, Minoshima S, Giordani B, et al. Cerebral metabolic differences in Parkinson's and Alzheimer's diseases matched for dementia severity. *J Nucl Med.* 1997;38:797-802.
26. Ito H, Kawashima R, Awata S, et al. Hypoperfusion in the limbic system and prefrontal cortex in depression: SPECT with anatomic standardization technique. *J Nucl Med.* 1996;37:410-414.
27. Reiman EM, Caselli RJ, Yun LS, et al. Preclinical evidence of Alzheimer's disease in persons homozygous for the e4 allele for apolipoprotein E. *N Engl J Med.* 1996;334:752-758.
28. Kuwabara H, Cumming P, Yasuhara Y, et al. Regional striatal DOPA transport and decarboxylase activity in Parkinson's disease. *J Nucl Med.* 1995;36:1226-1231.
29. Minoshima S, Frey KA, Koeppe RA, et al. A diagnostic approach in Alzheimer's disease using three-dimensional stereotactic surface projections of fluorine-18-FDG PET. *J Nucl Med.* 1995;36:1238-1248.
30. Minoshima S, Koeppe RA, Frey KA, Kuhl DE. Automatic standardization: linear scaling and nonlinear warping of functional brain images. *J Nucl Med.* 1994;35:1528-1537.
31. Slomka PJ, Hurwitz GA, Stephenson J, Craddock T. Automated alignment and sizing of myocardial stress and rest scans to three-dimensional normal templates using an image registration algorithm. *J Nucl Med.* 1995;36:1115-1122.
32. Slomka PJ, Hurwitz GA, Clement GS, Stephenson J. Three-dimensional demarcation of perfusion zones corresponding to specific coronary arteries: application for automated interpretation of myocardial SPECT. *J Nucl Med.* 1995;36:2120-2128.